Original Research

MR-Guided Sclerotherapy of Low-Flow Vascular Malformations Using T_2-Weighted Interrupted bSSFP (T_2W-iSSFP): Comparison of Pulse Sequences for Visualization and Needle Guidance

Di Xu, MS,[1] Daniel A. Herzka, PhD,[1] Wesley D. Gilson, PhD,[2] Elliot R. McVeigh, PhD,[1] Jonathan S. Lewin, MD,[3] and Clifford R. Weiss, MD[3]*

Purpose: Image-guided treatment of low-flow vascular (venous or lymphatic) malformations presents a challenging visualization problem, regardless of the imaging modality being used for guidance. The purpose of this study was to employ a new magnetic resonance imaging (MRI) sequence, T_2-weighted interrupted balanced steady-state free precession (T_2W-iSSFP), for real-time image guidance of needle insertion.

Materials and Methods: T_2W-iSSFP uses variable flip angle balanced steady-state free precession (bSSFP, a.k.a. SSFP) to establish T_2-weighting and fat suppression. Swine ($n = 3$) and patients ($n = 4$, three female, all with venous malformations) were enrolled in the assessment. T_2-weighted turbo spin echo (T_2-TSE) with spectral adiabatic inversion recovery (SPAIR), SPAIR-T_2-TSE or T_2-TSE for short, was used as the reference. T_2-weighted half Fourier acquired single shot turbo spin echo (T_2-HASTE) with SPAIR (SPAIR-T_2-HASTE, T_2-HASTE for short), fat saturated bSSFP (FS-SSFP), and T_2W-iSSFP were imaged. Numeric metrics, namely, contrast-to-noise ratio (CNR) efficiency (CNR divided by the square root of acquisition time) and local sharpness (the reciprocal of edge width), were used to assess image quality. MR-guided sclerotherapy was performed on the same patients using real-time T_2W-iSSFP to guide needle insertion.

Results: Comparing the visualization of needles in the images of swine, the local sharpness (mm^{-1}) was: 0.21 ± 0.06 (T_2-HASTE), 0.48 ± 0.02 (FS-SSFP), and 0.49 ± 0.03 (T_2W-iSSFP). T_2W-iSSFP is higher than T_2-HASTE ($P < 0.001$). For the patient images, their CNR efficiencies were: 797 ± 66 (T_2-HASTE), 281 ± 44 (FS-SSFP), and 860 ± 29 (T_2W-iSSFP). T_2W-iSSFP is higher than FS-SSFP ($P < 0.02$). The frame rate of T_2W-iSSFP was 2.5–3.5 frames per second. All MR-guided sclerotherapy procedures were successful, with all needles (six punctures) placed in the targets.

Conclusion: T_2W-iSSFP provides effective lesion identification and needle visualization. This new pulse sequence can be used for MR-guided sclerotherapy of low-flow vascular malformations. It may have potential use in other MR-guided procedures where heavily T_2-weighted real-time images are needed.

Key Words: low-flow vascular malformations; MR-guided sclerotherapy; real-time guidance of needle placement; T_2-weighted fat suppressed magnetic resonance imaging; real-time MR imaging
J. Magn. Reson. Imaging 2015;41:525–535.

LOW-FLOW VASCULAR MALFORMATIONS, which are classified as venous malformations (VMs) and lymphatic malformations (LMs), are congenital lesions that mostly affect children and young adults (1). These lesions, which often cause pain, cosmetic problems, functional deficits, or, in the case of lymphatic malformations, recurrent infections, are typically treated percutaneously using sclerotherapy. The treatment procedure consists of two parts. Most commonly, ultrasound (US) is first used to identify the target and guide needle insertion. Flow is then assessed and sclerosant administration is monitored using x-ray fluoroscopy. This involves injection of iodinated contrast in order to identify both the flow within the lesion, and the existence and character of any draining veins. However, certain lesions cannot be accurately targeted using US (2–4). Typically, these include lesions that lie deep within the body, are located within or behind bone, or lie beneath previously treated lesions that are now scar and fibrotic. Additionally, most patients require multiple treatment sessions, repeatedly exposing patients (many of whom

[1]Department of Biomedical Engineering, Johns Hopkins University School of Medicine, Baltimore, Maryland, USA.
[2]Center for Applied Medical Imaging, Imaging & Computer Vision, Siemens, Corporate Technology, Baltimore, Maryland, USA.
[3]Department of Radiology, Johns Hopkins University School of Medicine, Baltimore, Maryland, USA.
Contract grant sponsor: NIH; Contract grant numbers: UL1RR025005, JHU ICTR ATIP; Contract grant sponsor: Siemens Healthcare.
*Address reprint requests to: C.R.W., Assistant Professor of Radiology, Surgery and Biomedical Engineering, Interventional Radiology Center, Sheikh Zayed Tower, Suite 7203, Johns Hopkins Hospital, Baltimore, MD 21287. E-mail: cweiss@jhmi.edu
Received August 20, 2013; Accepted November 22, 2013.
DOI 10.1002/jmri.24552
View this article online at wileyonlinelibrary.com.

are children or women of childbearing age) and clinical staff to ionizing radiation.

Magnetic resonance imaging (MRI)-guided sclerotherapy has the potential to be a safer alternative to these modalities by eliminating radiation exposure and by providing better visualization of the lesions, as well as surrounding soft tissues and critical structures. The procedural steps of MR-guided sclerotherapy can be found in the MR-guided Sclerotherapy in Patients subsection of the Materials and Methods. T_2-turbo spin echo (TSE) combined with fat suppression by spectral adiabatic inversion recovery (SPAIR) is the reference technique for diagnostic visualization of VMs and LMs (5,6). The malformations are clearly detectable as hyperintensities due to the heavy T_2-weighting and sharp images. However, the acquisition speed for SPAIR T_2-TSE is too slow for real-time needle guidance. Commercially available real-time sequences exist, but either produce heavily T_2-weighted images with blurry, distorted edges for tissues with longer T_2 times (T_2-half Fourier acquired single shot turbo spin echo [HASTE]) (7,8) or produce sharp images with poor T_2 contrast leading to poor target identification (balanced steady-state free precession [bSSFP]) (9,10).

In this study, a new sequence, termed T_2W-iSSFP, was implemented. Moreover, its feasibility in the context of needle guidance of MR-guided sclerotherapy was evaluated. This pulse sequence was designed for the real-time guidance of needle insertion, and combines the desired speed, image sharpness, and tissue contrast needed for high-quality visualization of lesions, surrounding critical structures, and moving needles.

MATERIALS AND METHODS

MR Sequence

T_2W-iSSFP generates simultaneous T_2 contrast and fat suppression by combining two established techniques: T_2-weighted transition into driven equilibrium (T_2-TIDE, T_2-weighting) (11) and fat saturated-TIDE (FS-TIDE, fat suppression) (12). The combination is achieved by lengthening the radiofrequency (RF) pulses and has been previously described (13). This sequence is a variable flip angle bSSFP sequence, using a single-shot real-time imaging protocol (13).

Each train begins with an $\alpha/2$-TR/2 pulse ($\alpha/2 = 90^\circ$) (14) followed by a number ($N_{RF} = 35$) of high flip angle (typically 180°) RF refocusing pulses to generate T_2 contrast. In these 35 RFs, 20 are used for magnetization preparation. Hence, data sampling begins at $N_{RF} = 21$ and proceeds with centric phase-encoding, eg, k = 0,−1,+1,−2,+2,..., to the edge of *k*-space throughout the imaging train. After, the flip angles are progressively decreased to the nominal imaging flip angle (α_{ssfp}) that is used for bSSFP imaging, typically $\alpha_{ssfp} = 60^\circ$, in a quadratic manner, smoothly transitioning towards steady-state and reducing artifacts that compromise image sharpness (11,15). At the end of the imaging train, magnetization is restored by an $\alpha/2$ pulse followed by a gradient crusher, storing the spins in the z-axis and removing the residual transverse coherences (16). To accelerate the imaging, generalized autocalibrating partially parallel acquisitions (GRAPPA) is applied with a 2-fold undersampling (17), reducing the net number of TRs in the train (13).

The flip angle of the RF refocusing pulses at the beginning of the T_2W-iSSFP train is the maximum flip angle (max flip angle, α_{max}) of the variable flip angle train. This max flip angle can be changed between the nominal imaging flip angle (60°) and 180°. Low max flip angle T_2W-iSSFP has the max flip angle the same as α_{ssfp} (typically, $\alpha_{max} = \alpha_{ssfp} = 60^\circ$) and can produce bSSFP image contrast ($\sim T_1/T_2$), with signals in soft tissue. High max flip angle T_2W-iSSFP has $\alpha_{max} = 180^\circ$ and can produce T_2-weighted fat-suppressed images. Note that low max flip angle T_2W-iSSFP is actually imaging at the transition phase of bSSFP sequence (15).

Study Phases

To safely deploy T_2W-iSSFP during interventional procedures and investigate the feasibility of using T_2W-iSSFP in MR-guided sclerotherapy, this study had three phases: 1) assessment of needle visualization during insertion; 2) assessment of the detectability of lesions and surrounding critical structures; and 3) clinical evaluation of MR-guided sclerotherapy in patients with venous malformations. All experiments/procedures were performed at 1.5T using a wide-bore scanner (MAGNETOM Espree, Siemens Healthcare, Erlangen, Germany).

Needle Visualization in Swine

All animal experiments were performed with the approval of the local Animal Care and Use Committee. Swine ($n = 3$) were anesthetized and placed in the magnet in the head-first prone position. T_2W-iSSFP was used during and after needle placement. Twenty-two gauge MR-compatible needles (10–15 cm in length, MREye, Cook Medical, Bloomington, IN) were inserted through the flank into the renal collecting system of one or both kidneys while imaging using real-time T_2W-iSSFP.

With the needles in place, four imaging sequences were acquired to assess their ability to visualize the inserted needle: T_2-TSE, T_2W-iSSFP, FS-SSFP, and T_2-HASTE. T_2-TSE was used as the reference for visualization as a nonreal-time imaging sequence. The images of the sequences were compared, as stated in the "Assessment" section. All of the sequences were performed using oblique axial and oblique sagittal imaging plane positions that were parallel to the needle. Phase encoding was either along the y axis or along the z axis. The specific absorption rate (SAR) of each sequence was also recorded.

Visualization of Lesions and Surrounding Critical Structures in Patients

Under Institutional Review Board (IRB) approval and informed consent, four patients (ages 27–54, three

Table 1
Summary of the Data of the Four Interventions on the Four Patients

Patient #	Age	Sex	# of Lesions Targeted	# of Lesions for Testing Visualization	Lesion Location(s)	Coils Used
1	33	F	1	1	Right Side Chest Wall	Single Loop
2	41	F	2	6*	Pelvis, Abdomen	Phased Array
3	27	F	1	1	Left Hand	Single Loop
4	54	M	2	2	Bilateral Trapezius Muscles	Single Loop

*Six VMs are listed. Two VMs were in her pelvis, both of them were the targeted lesions of the intervention. Also, we scanned the other four abdominal VMs in two diagnostic imaging sessions taken in two different days. These four abdominal VMs were not treated in the interventions listed in this table.

females) with venous malformations were prospectively enrolled in the second and third phases of the study, which were the diagnostic imaging sections and MR-guided sclerotherapy, respectively. Inclusion criteria were: adults patients (>18 years old), with low-flow vascular malformations and with an actual or predicted inability to visualize their malformations using ultrasound. All interventional procedures were conducted by two interventional radiologists with extensive experience treating vascular malformations using both standard and MRI techniques (C.R.W. 8 years, J.S.L. 20 years). General anesthesia was used for all sclerotherapy procedures.

The four patients had a total of six imaging sessions in the second phase of the study (image quality in vivo) (Table 1). Patient #1 was a 33-year-old woman with a small residual VM in her right side chest wall. Patient #2 was a 41-year-old woman with multiple large VMs throughout her abdomen and pelvis. Patient #3 was a 27-year-old woman with a small residual VM in her left hand. Patient #4 was a 54-year-old man with small bilateral trapezius VMs.

Three patients (patients #1, 3, and 4) had one imaging session only. Patient #2 underwent three different imaging sessions of the VMs. Particularly, she had two imaging sessions of her abdomen (two VMs each session, hence four VMs in total) and one session of her pelvis (two VMs) (Table 1).

In all of these imaging sessions, T_2-TSE (reference), T_2W-iSSFP, FS-SSFP, and T_2-HASTE were used. Two abdominal scans of patient #2 were taken as part of two separate diagnostic scans without anesthesia. The remaining four scans were acquired as part of the diagnostic scans taken for planning purposes prior to interventions.

For the four abdominal and pelvic scans, a 6-channel abdominal phased array was used in conjunction with the in-table spine array. For trapezius, chest wall, and hand scans, a 19-cm single loop flex coil was applied in conjunction with the in-table spine array.

MR-Guided Sclerotherapy in Patients

Four MR-guided sclerotherapy procedures were performed using T_2W-iSSFP to guide needle insertion. Twenty and 22 gauge MR-compatible needles with lengths of either 10 or 20 cm were used (Cook Medical; E-Z-EM, Westbury, NY). Both SAR and deposited RF energy were monitored and recorded by the MR scanner system.

For each procedure, planning MR was performed using T_2-TSE with slice thickness of 3 mm, in three stacks of slices: axial, coronal, and sagittal. The most appropriate stack of images was selected for needle insertion trajectory planning, which determined the skin entry point and the needle insertion angle and depth. Next, the skin entry sites were localized by moving a syringe filled with saline along the skin surface during real-time imaging using T_2W-iSSFP (18). Once the syringe tip corresponded to the desired skin entry site and angle, this site was marked, and the initial puncture of skin was performed outside the bore of the magnet.

The patient was then moved inside the bore of the magnet for needle placement under real-time MR guidance. The needle was guided into the malformation using continuous visualization with real-time T_2W-iSSFP imaging (5 mm thickness, 0.3–0.4 sec per slice, 3–5 parallel slices), until the tip of the needle was clearly seen within the targeted lesion. Multiple imaging planes, including oblique axial, oblique coronal, and oblique sagittal, were used. While inserting the needle, low ($\alpha_{max} = 60°$) and high ($\alpha_{max} = 180°$)

Table 2
Imaging Protocols for the Experiments of Animals and Patients With VMs

	TSE	HASTE	FS-SSFP	T_2W-iSSFP
Field of View (mm)	300	300	300	300
Slice Thickness (mm)	5	5	5	5
Resolution (mm^2)	1.6 × 1.6	1.6 × 1.6	1.6 × 1.6	1.6 × 1.6
Acquisition Time (s)	20	2	0.7	0.7
TE/TR (ms)	90/5000	91/2000	1.85/3.7	2.25/4.5
Echo Spacing (ms)	15.8	7.5	3.7	4.5
Flip Angles	90°/180°	90°/180°	60°	90°/180°/60°
Pixel Bandwidth (Hz/px)	100	195	810	868

max flip angles of T_2W-iSSFP were alternatively selected to emphasize visualization of either the malformation or the needle as requested by the interventional radiologist. Access of the targeted lesion was confirmed by T_2-TSE and by blood return.

Once confirmed, gadolinium-doped saline was delivered through the needle for flow assessment. Next, the sclerosant was administered (19). The flow assessment and the injection of sclerosant were monitored by a dynamic "thick slab" fast low angle shot sequence (FLASH, with subtraction, <2 frames/s) or by a 3–5 parallel slices (5 mm) 2D FLASH. After the sclerosant was administered, the lesion was scanned using T_1-weighted volumetric interpolated breath-hold imaging (VIBE) (20), in order to visualize the doped sclerosant filling in the targeted VM and to serve as a final confirmation of accurate sclerosant delivery. Imaging protocols of T_2-TSE, T_2-HASTE, FS-SSFP, and T_2W-iSSFP in all of the experiments are listed in Table 2.

Assessment

To quantitatively evaluate the three competing real-time sequences, two numerical metrics were used. Contrast-to-noise ratio (CNR) efficiency, which is the CNR divided by the square root of imaging time, was used for evaluating image contrast between VMs and background tissue such as muscle and fat (21). CNRs were measured by $\frac{I_{VM}-I_{muscle}}{noise}$ and $\frac{I_{VM}-I_{fat}}{noise}$ for VMs vs. muscle and VMs vs. fat, respectively; where I_{VM}, I_{muscle}, and I_{fat} were measured as the mean intensities of the regions of interest (ROIs) placed on the VMs, muscle, and fat, respectively. Noise was measured as the standard deviations of the ROIs placed outside the body. To fairly compare the CNRs, parallel imaging was disabled when acquiring images for measuring CNRs. Further, the CNRs were corrected for different pixel bandwidth (BW) and partial Fourier factors (PFF) as $\sqrt{\frac{BW}{PFF}}CNR$ (11).

Local sharpness was used for assessing the sharpness (22). This metric is defined as the reciprocal of edge width, which is the distance between the image intensity local maxima to the local minima near the edge of the evaluation targets (which can be either VMs or needles). To calculate the edge width, the distance between the local maxima and minima was measured by the intensity profile of a line placed perpendicular to the edge of the target. The CNR efficiency and the local sharpness of VMs were measured from the images obtained from the experiments in "Visualization of Lesions and Surrounding Critical Structures in Patients," and the local sharpness of needles were measured from the images obtained from the experiments in "Needle Visualization in Swine." For comparison purposes, the same window/level was used for display and calculation of image metrics from the same experiment.

Once the numerical metrics were collected, statistical tests were applied. The metrics of the images sampled by the same sequence were collected into one group. Therefore, three groups of data were collected for each metric. The Jarque-Bera test was applied on each group to determine whether it follows Gaussian distribution (23). Next, one-way analysis of variance (ANOVA) (24) was performed on those three groups to determine whether any of the three groups (ie, sequences) had significantly better or worse performances than the others.

Qualitative assessment was also performed (Table 3). T_2-TSE, T_2-HASTE, FS-SSFP, and T_2W-iSSFP were assessed in five aspects: image contrast, imaging speed, image sharpness, flexibility, and SAR safety. For all of these aspects, the performance of these four sequences was rated as bad, uncertain, good, or very good by the consensus from two evaluators: D.A.H. (MR physicist/imaging scientist 15 years of experience) and C.R.W. (interventional radiologist, 16 years of experience). Particularly, imaging speed was assessed by the frame rate, and SAR safety was assessed by SAR and the safe standards. Image contrast and image sharpness were visually evaluated from the images of those four sequences. Flexibility was assessed by the number of parameters needed to be modified to change the image contrast. For example, T_2W-iSSFP could change its image contrast by only modifying its α_{max}, as shown in the results of "Needle Visualization in Swine" and "MR-guided Sclerotherapy in Patients."

RESULTS

Needle Visualization in Swine

In all of the three experiments (four punctures in total), all needles were placed into the targeted renal collecting system using T_2W-iSSFP for image guidance. T_2W-iSSFP had a frame rate of 2.5–3.5 frames per second (fps), which was adequate for real-time needle guidance. Additionally, T_2W-iSSFP provided different contrasts, by changing the max flip angle, for different needs at different points in the procedure. Low max flip angle T_2W-iSSFP enhanced visualization of the needles. (Fig. 1c) High max flip angle T_2W-iSSFP emphasized visualization of the renal collecting system, due to the long T_2 of the fluid (Fig. 1e).

The images in Fig. 1 were acquired after needle placement. Both T_2W-iSSFP (high α_{max}) and T_2-HASTE clearly identified the renal collecting system due to their prominent T_2-weighting. Conversely, the $\sim T_2/T_1$ weighting of FS-SSFP generated visibly lower contrast between the renal collecting tube and surrounding tissues (Fig. 1).

FS-SSFP and T_2W-iSSFP (low α_{max}) clearly showed the needles, as well as boundaries between the needle and the surrounding muscle/fat; whereas T_2-HASTE yielded images with blurry and fuzzy needle edges (Fig. 1d).

Finally, both T_2W-iSSFP and FS-SSFP had lower SAR than T_2-HASTE (T_2-HASTE: 1.6 ± 0.1 W/kg, FS-SSFP: 1.1 ± 0.3 W/kg, T_2W-iSSFP: 1.3 ± 0.1 W/kg).

Visualization of Lesions and Surrounding Critical Structures in Patients

Using T_2-TSE as the reference, all lesions (10/10, all venous malformations, details in Table 1) were

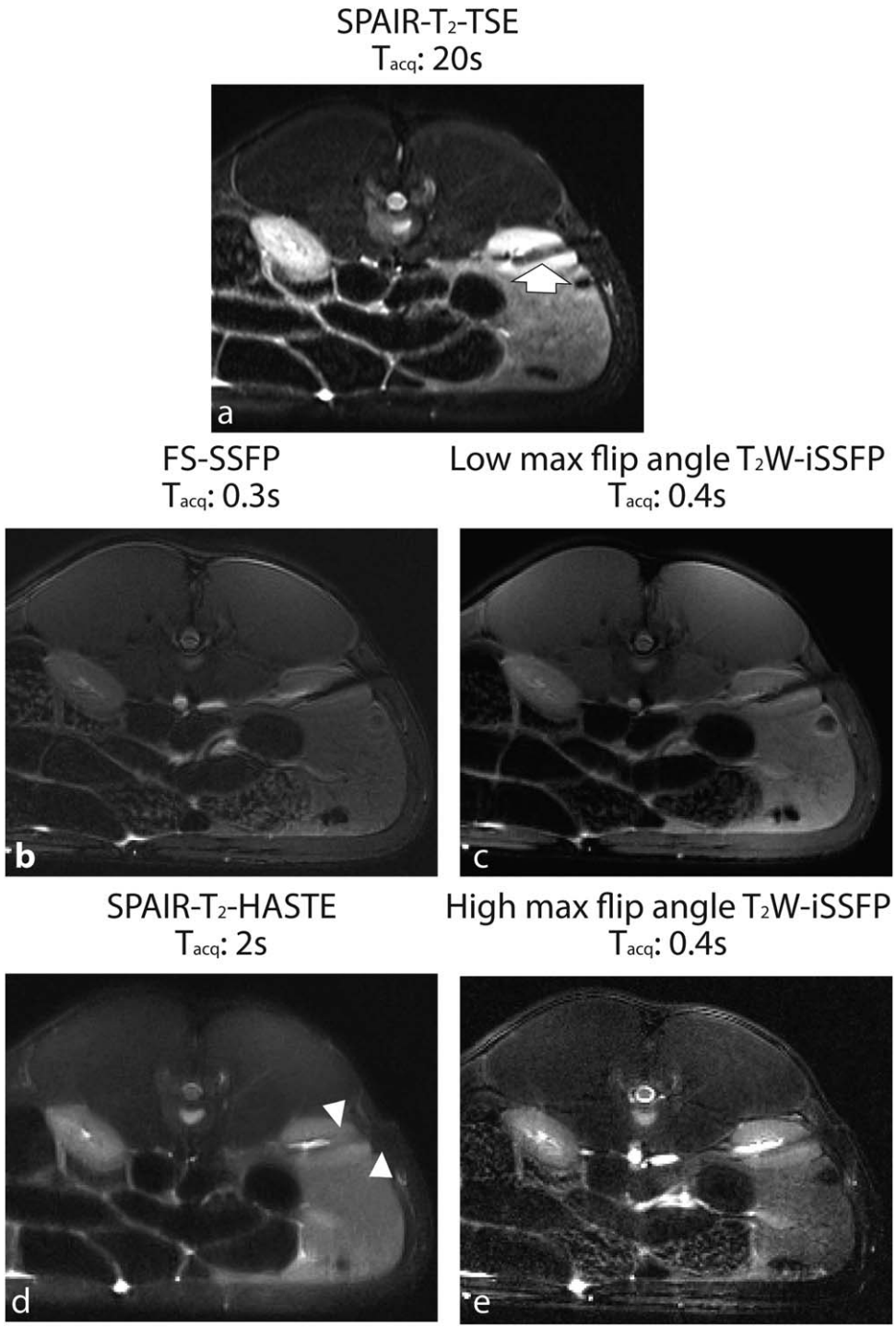

Figure 1. Images from a swine after a needle successfully inserted using T_2W-iSSFP as the guidance. Multiple imaging sequences are shown, along with the acquisition time for each image (T_{acq}). To ensure the needle was visible in all planes, images were acquired with breath-holds controlled by a ventilator. **a:** T_2-TSE is the reference for identifying the renal collecting system and for delineating the needle. Although it clearly shows the needle (arrow in a) and offers the best image quality, it is too slow for real-time needle guidance (20-sec T_{acq}). **(b)** FS-SSFP, **(d)** T_2-HASTE, **(c)** low, and **(e)** high max flip angle T_2W-iSSFP were used for comparison. The needle is clearly depicted in (a,b,c,e), whereas (c) T_2-HASTE shows a blurry needle (arrowheads). In addition, the needle can also be visualized in the muscle in both (b,c). Conversely (a,d,e) clearly identify the renal collecting system and can distinguish it from surrounding renal tissue, yet (b) barely distinguishes the renal collecting system from the surrounding renal tissue.

identified by both T_2-HASTE and T_2W-iSSFP; whereas FS-SSFP could only identify five of them. The lesions that were not identified by FS-SSFP were at different locations: two in bilateral trapezius muscle, one in the left hand, and the other two in the abdomen. All of them were indistinguishable from surrounding normal tissues (which were muscle, bowel, and tendon, depending on location) by FS-

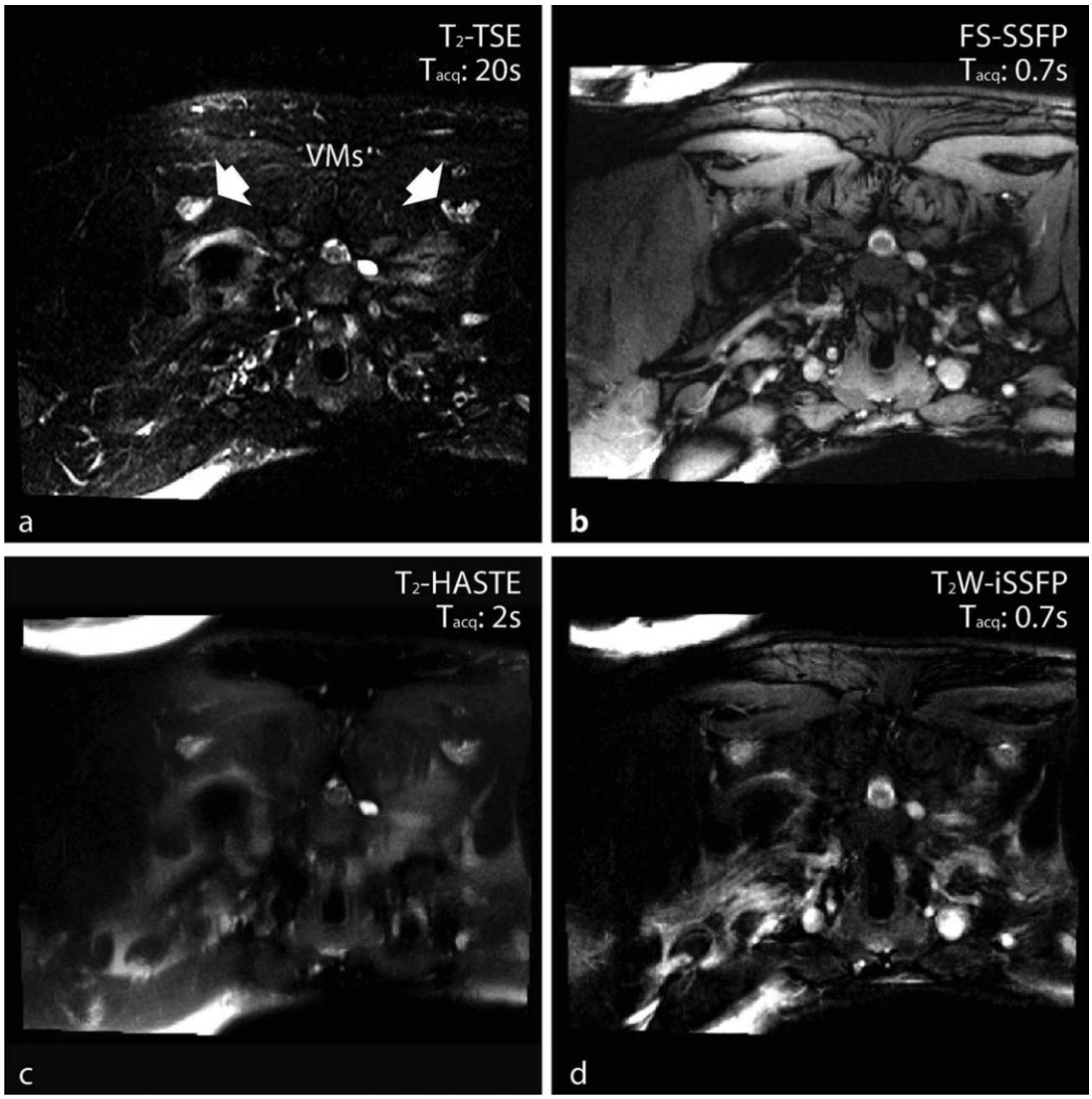

Figure 2. Images of a patient with VMs in his bilateral trapezius muscle (patient #4). **a:** T_2-TSE with SPAIR was used as the reference. (**b**) FS-SSFP, (**c**) T_2-HASTE, and (**d**) T_2W-iSSFP ($\alpha_{max} = 180^\circ$) are shown for comparison. Two VMs (arrows in a) are clearly seen in (a,c,d). FS-SSFP (b) was unable to distinguish these VMs from the surrounding normal trapezius muscle. T_2-HASTE (c) presents blurry VM margin and ambiguous boundaries of the surrounding normal blood vessels.

SSFP due to poor T_2 contrast. Some representative cases are shown (patients #4 and #2 in Figs. 2 and 3, respectively).

In terms of the CNR efficiency (of both VMs vs. muscle and VMs vs. fat), T_2W-iSSFP and T_2-HASTE were similar, and both were significantly higher than FS-SSFP (VMs vs. muscle: $P < 0.02$, VMs vs. fat $P < 0.01$). A bar graph of CNR efficiencies is shown in Fig. 4a: VM vs. muscle: 797 ± 66 (T_2-HASTE), 281 ± 44 (FS-SSFP), and 860 ± 29 (T_2W-iSSFP); VM vs. fat: 909 ± 33 (T_2-HASTE), 185 ± 50 (FS-SSFP), and 862 ± 40 (T_2W-iSSFP). In terms of the local sharpness (of both VMs and needles), T_2W-iSSFP and FS-SSFP were similar, and both were significantly sharper than T_2-HASTE (VMs: $P < 0.001$, needles: $P < 0.001$). A bar graph of local sharpness is shown in Fig. 4b: VMs: 0.13 ± 0.04 (T_2-HASTE), 0.31 ± 0.04 (FS-SSFP), and 0.3 ± 0.03 (T_2W-iSSFP); needles: 0.21 ± 0.06 (T_2-HASTE), 0.48 ± 0.02 (FS-SSFP), and 0.49 ± 0.03 (T_2W-iSSFP).

Sclerotherapy in Patients

All MR-guided sclerotherapy procedures using T_2W-iSSFP were successful. Specifically, all needles (six punctures) were placed in the targeted lesions, allowing sclerosant delivery. The needle placements were confirmed by post-insertion T_2-TSE, and the sclerosant deliveries were confirmed by post-contrast VIBE. The post-insertion T_2-TSE and post-contrast VIBE images of each patient are shown in Figs. 5 and 6. These images confirmed the success of needle placements and sclerosant deliveries. Additionally, the SARs of T_2W-iSSFP were 1.7 ± 0.2 W/kg (deposited energy: 201 ± 40W), which were within tolerable values.

Results of the qualitative assessment of all four sequences (including T_2-TSE) are shown in Table 3. Even though T_2W-iSSFP is not the top performer in all categories, it has relatively high performance in all of these metrics.

A representative case (patient #1) is shown in Fig. 5. This patient had a residual VM in the right

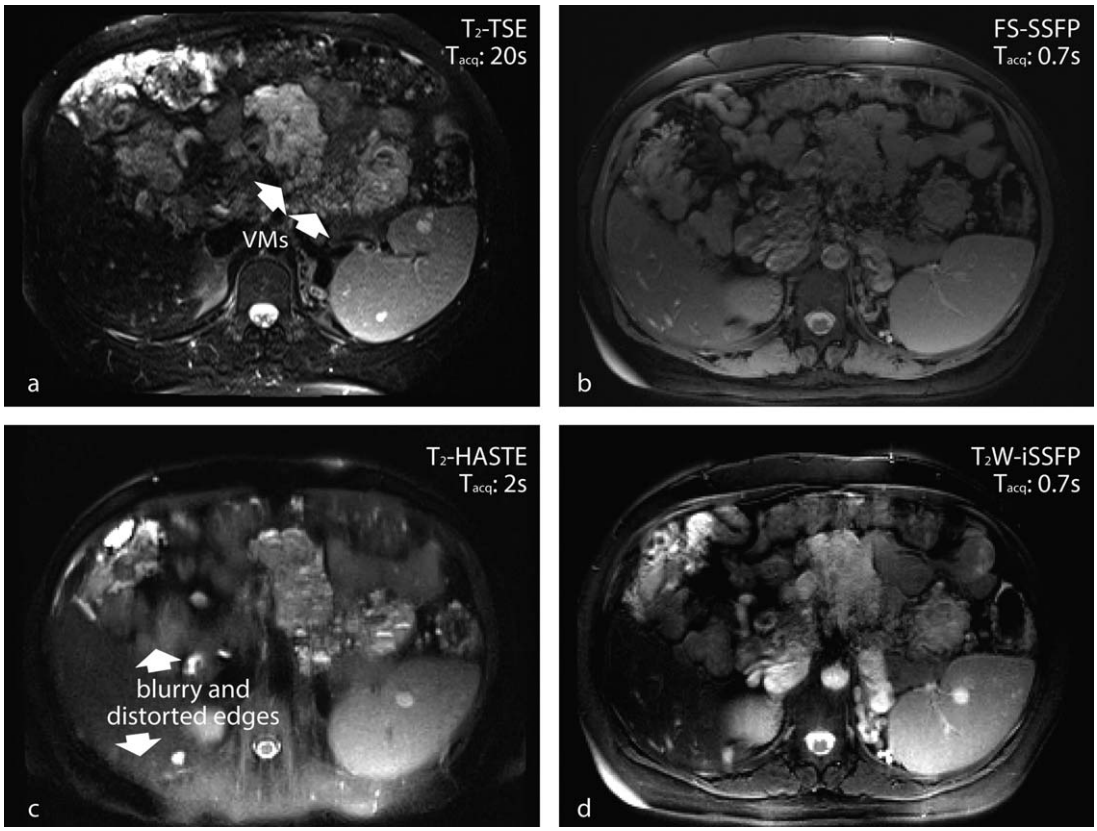

Figure 3. Images of the abdomen of patient #2. **a:** T_2-TSE is the reference. Real-time sequences, **(b)** FS-SSFP, **(c)** T_2-HASTE, and **(d)** T_2W-iSSFP are shown for assessment. Two malformations (arrows in a) are clearly identified in (a,c,d). However, those lesions cannot be found in SSFP (b). On the other hand, HASTE (c) presents blurry depiction of the bowel and the normal blood vessels. Those surrounding critical structures are very dangerous if punctured when inserting needles.

chest wall. Before this MR-guided procedure, standard percutaneous techniques using ultrasound were attempted twice, and both of them were unsuccessful. The room setup is shown in Fig. 5a. Real-time MR video was incorporated with an interventional guidance visualization software (interactive front-end [IFE], Siemens Corporate Research, Princeton, NJ) (25) and displayed on an in-room projector. Initially, when the needle was in the muscle and the fat, low max flip angle T_2W-iSSFP was used for needle visualization (Fig. 5b). When the needle approached the VM, high max flip angle T_2W-iSSFP was used. It increased lesion contrast and conspicuity and aided accurate needle tip placement within the lesion (Fig. 5c). During needle insertion, images were produced with a relatively fast frame rate (2.5–3.5 fps), which permitted real-time needle guidance. Follow-up T_2-TSE and T_1-VIBE confirmed the success of the needle placement and the sclerosant delivery, respectively (Fig. 5d,e).

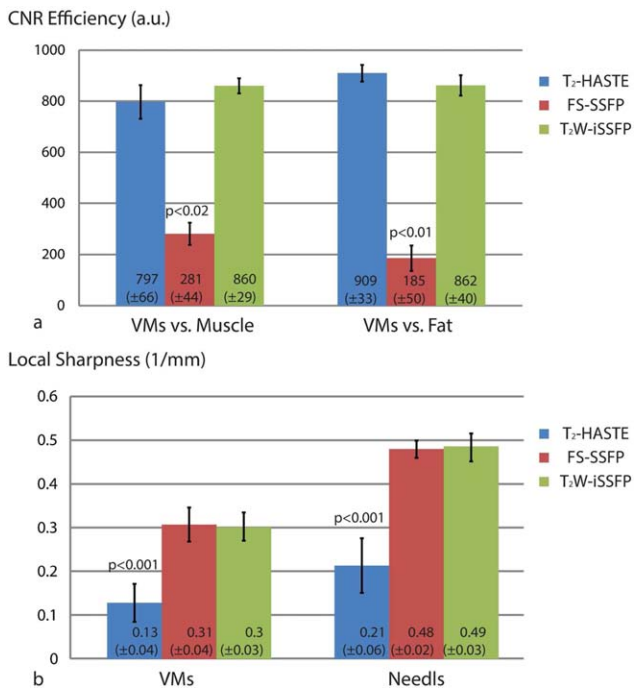

Figure 4. Graphs comparing the image contrast and the image sharpness of T_2-HASTE (blue), FS-SSFP (red), and T_2W-iSSFP (green), by two numerical metrics: **(a)** CNR efficiency (for image contrast) and **(b)** local sharpness (for image sharpness). [Color figure can be viewed in the online issue, which is available at wileyonlinelibrary.com.]

DISCUSSION

MR-guided VM sclerotherapy needs fast imaging for real-time guidance. The "real-time" guidance concept means an acceptable frame rate of continuous image acquisition (typically >1 fps) and a short delay of image display (<200 msec), all during needle insertion. Also, the procedure needs a safe guidance approach with high image quality, including heavy T_2

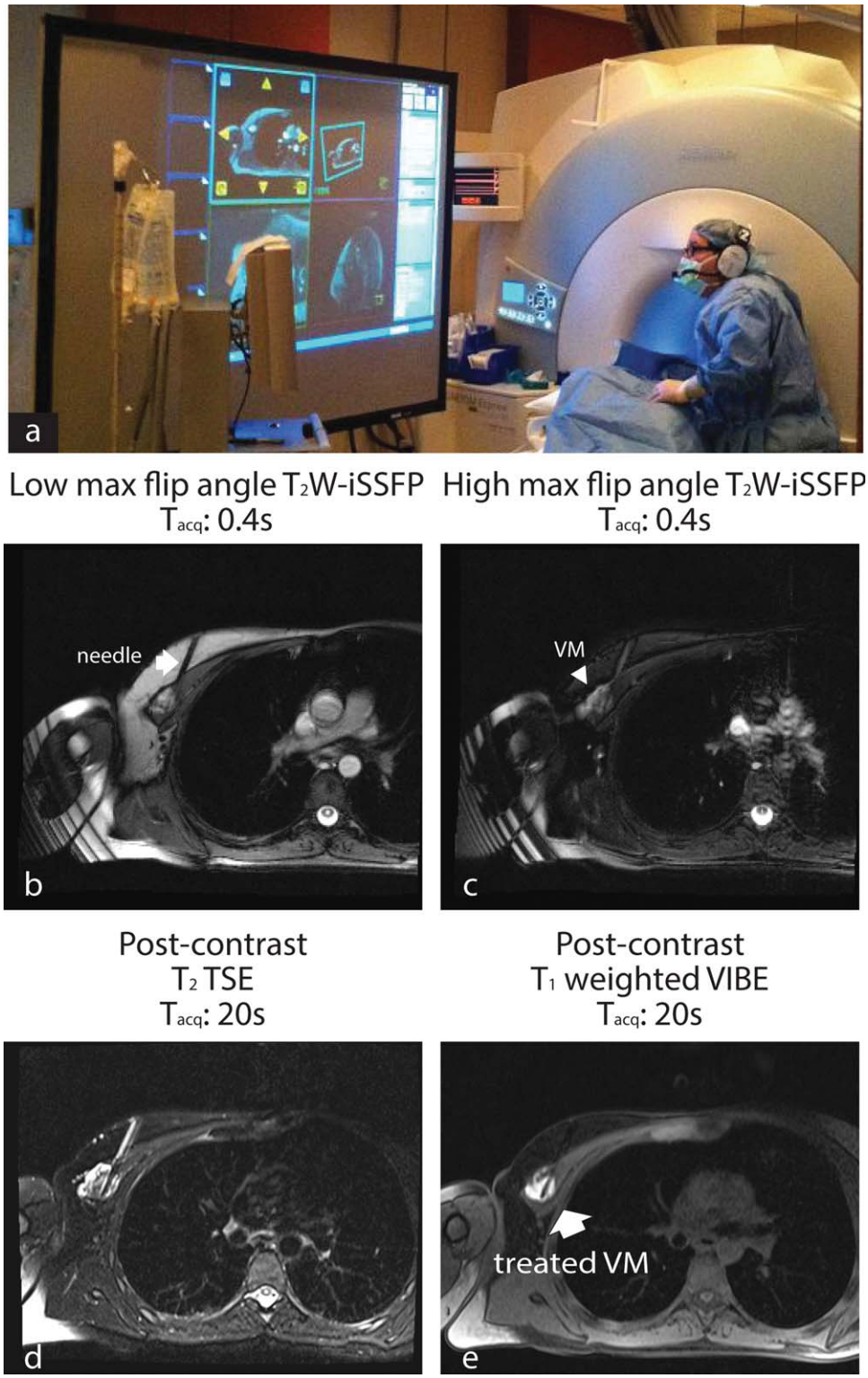

Figure 5. An example of a MR-guided sclerotherapy using T_2W-iSSFP. This patient (#1) had a residual VM in her chest wall, causing pain. Before this procedure, we tried twice using ultrasound to access this lesion, unsuccessfully. **a:** Procedural room setup of this MR-guided sclerotherapy is shown. Real-time MR video was integrated into an interventional guidance visualization software (25) and displayed on an in-room projector. **(b)** High and **(c)** low max flip angle real-time T_2W-iSSFP images are shown. They were sampled during the needle insertion. Real-time T_2W-iSSFP offers heavily T_2-weighting and high image quality to visualize the lesion and its extent, as well as the surrounding critical structures such as the normal blood vessels and the lung. These critical structures should be avoided when inserting needles. High max flip angle T_2W-iSSFP provides heavily T_2-weighting for visualizing the VM emphatically (arrowhead in c). Low max flip angle T_2W-iSSFP emphasizes the depiction of the needle (the arrow in b) and the surrounding soft tissue. **(d)** Post-contrast T_2-TSE and **(e)** post-contrast T_1-weighted VIBE (20) demonstrate the success of the needle placement and the filling of the sclerosant (sodium tetradecyl sulfate).

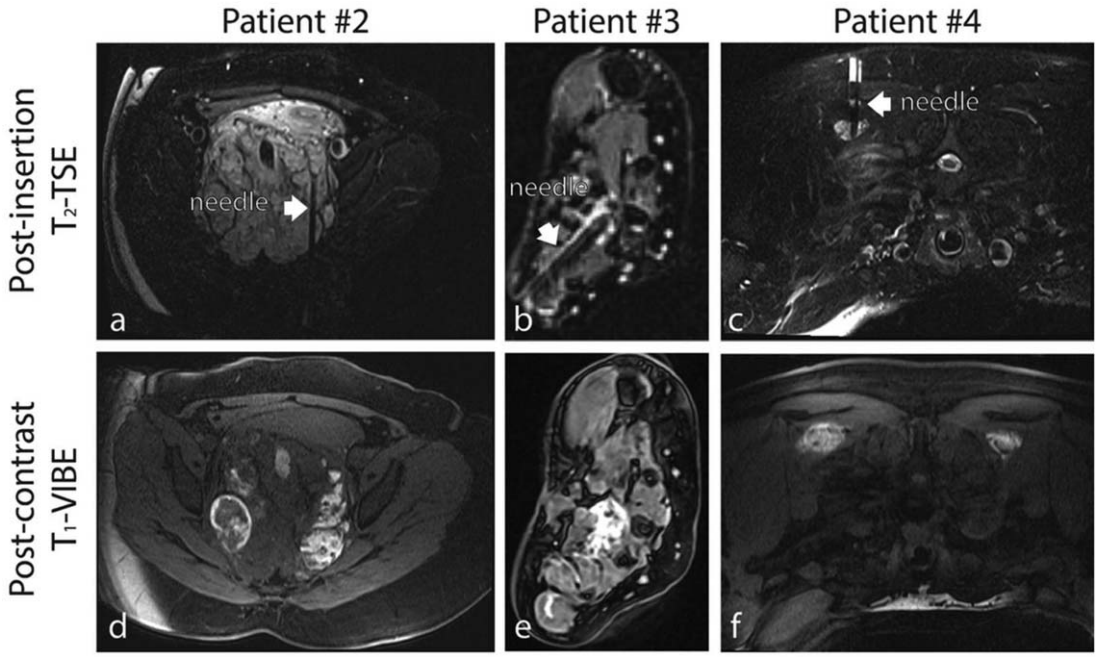

Figure 6. Depiction of post-insertion T_2-TSE **(a–c)** and post-contrast T_1-VIBE **(d–f)**. These images were from the MR-guided sclerotherapies using T_2W-iSSFP, and confirmed the needle placement (T_2-TSE) and the sclerosant administration (T_1-VIBE), respectively. a,d: From a patient (#2) with massive VM throughout her abdomen and pelvis. This treatment was deep in the pelvis, just adjacent to the rectum. Real-time T_2W-iSSFP provided excellent images for avoiding puncturing the rectum and the surrounding normal blood vessels. Patient #3 (b,e) had a VM in her hand. The VM was surrounded by nerves and tendons, and laid beneath extensive scar tissue from many previous surgeries and sclerotherapies. T_2W-iSSFP offered high-quality visualization of the VM extent, as well as facilitated the needle insertion to avoid those critical structures (nerves and tendons). Patient #4 had two VMs deep in the trapezius muscle. Ultrasound could not distinguish them from the surrounding muscle, whereas T_2W-iSSFP could identify these two lesions (Fig. 2d).

Table 3
Qualitative Assessment of the Existing MR Sequences for VMs Diagnostic and Interventional Procedures

	TSE	HASTE	SSFP	T_2W-iSSFP
Imaging Speed	−	+/−	++	+
SAR Safety	+	+	++	+
Image Contrast	++	+	−	+
Image Sharpness	++	−	++	+
Flexibility	+/−	+/−	+	++

We evaluated these sequences in the aspects of image contrast, imaging speed, image sharpness, flexibility, and SAR safety. T_2W-iSSFP shows high performance in all of these aspects, making it a suitable sequence for guiding needle insertion when T_2-weighted real-time imaging is needed. -: bad, +/-: uncertain, +: good, ++: very good.

contrast for lesion identification and sharp images for delineating needles and lesion margins. A flexible imaging sequence, which can adjust the degree of T_2-weighting, can help emphasize either needle visualization or target identification.

In this study, we demonstrated that T_2W-iSSFP can be used for real-time needle guidance of MR-guided sclerotherapy in patients. First of all, this sequence is sufficiently fast (2.5–3.5 fps) for real-time guidance. Also, it produces moderately low SAR, safe for guiding needle placement in patients. The SAR reduction to T_2-HASTE can be accounted for by the flip angle ramp and the nominal flip angle. Nevertheless, the increased imaging speed offsets some of the gains in SAR reduction.

Furthermore, T_2W-iSSFP is effective for identifying lesions, distinguishing surrounding critical structures, and visualizing needles. It offers high-quality images, which exhibit both strong T_2 contrast and high image sharpness. In terms of T_2 contrast, this sequence is similar to T_2-HASTE and is higher than FS-SSFP. In the aspect of image sharpness, T_2W-iSSFP is similar to FS-SSFP, and is sharper than T_2-HASTE. As a result, among all of the three competing sequences, T_2W-iSSFP offers the best overall image quality, the closest to T_2-TSE. Since T_2-TSE is too slow for real-time needle guidance, T_2W-iSSFP is the best sequence for guiding needle insertion.

In addition, T_2W-iSSFP is flexible. This sequence can adjust the degree of T_2 contrast by changing the maximum flip angle. A low flip angle can be useful for visualizing needles entering the fat and muscle layers when initially inserting needles. This is especially important when there is a thick layer of fat and muscle between the skin and the targeted lesion. When the needle approaches the VM, the contrast can be modified by changing the maximum flip angle to 180°, which emphasizes the targeted lesion.

Several limitations exist in this study. First of all, only one type of needle and two imaging planes were used in the animal experiments. However, using T_2W-iSSFP in the MR-guided sclerotherapy of patients,

needles from two vendors, with different gauges and lengths, were used; multiple imaging planes, including oblique axial, oblique coronal, and oblique sagittal were scanned. Previous study has investigated the needle visualization of multiple types and sizes needles and by various sequences, including SSFP-based sequences (29). SSFP sequence shows relatively high performance over other conventional sequences. Hence, it was used to compare the needle visualization with T_2W-iSSFP. Second, the images used for image quality assessment were sampled after the needles were positioned in the targets. Comparing images with moving needles may be more appropriate to assess those real-time sequences. In addition, the number of cases is insufficient to assess the clinical outcome of using T_2W-iSSFP in MR-guided sclerotherapy for the treatment of VMs. Instead, this study evaluated the feasibility of T_2W-iSSFP in MR-guided sclerotherapy procedures. Further studies for assessing outcome (eg, procedure time and treatment results) are needed.

T_2W-iSSFP was not compared with other T_2-weighted sequences in the literature. These sequences include T_2-TIDE, RE-TOSSI, and T_2-VAPSIF, among others (11,30,31). Although they have yet to be demonstrated, they could potentially be applied to needle guidance. However, RE-TOSSI and T_2-VAPSIF have not been designed to achieve fat suppression, which is valuable for distinguishing lesions with surrounding fatty tissue. Moreover, these techniques are not commercially available and have yet to be applied to the needle guidance of MR-guided sclerotherapy. Hence, it is difficult to make fair comparisons between these sequences, as differences in implementation could lead to unintended differences in performance relative to the published version. Additionally, it is not feasible to submit patients to extended imaging sessions to explore these different techniques for such a comparison. We chose T_2-HASTE and FS-SSFP as the standards since they have been used for needle guidance of MR-guided sclerotherapy for treating low-flow vascular malformations. A more comprehensive comparison with these techniques may be necessary.

Unlike T_2-TIDE, which uses partial Fourier encoding with linear phase encode ordering (11), T_2W-iSSFP uses centric ordering with full sampling in the k_y direction. Although partial Fourier appears to be more efficient, as it requires fewer phase encodes per image, using centric phase-encoding avoids the additional blurring associated with half-Fourier methods. As images already suffer from a T_2-dependent filtering effect due to T_2 decay and transition into steady-state (32), any additional loss in image quality could compromise needle visualization.

In conclusion, T_2W-iSSFP is a fast imaging sequence that produces significant T_2-weighting and fat suppression for visualizing lesions, acquires sharp images for visualizing needles, and offers adjustable contrast with simple changes in maximum flip angle. This work shows it is safe and feasible to use this sequence to effectively guide the needle insertion of MR-guided sclerotherapy for VM treatment. T_2W-iSSFP may also be used in other interventional procedures where real-time T_2-weighted imaging is needed (eg, liver biopsy and percutaneous nephrostomy).

REFERENCES

1. Legiehn GM, Heran M. A step-by-step practical approach to imaging diagnosis and interventional radiologic therapy in vascular malformations. Semin Interv Radiol 2010;27:209.
2. Boll DT, Merkle EM, Lewin JS. Low-flow vascular malformations: MR-guided percutaneous sclerotherapy in qualitative and quantitative assessment of therapy and outcome. Radiology 2004;233: 376–384.
3. Andreisek G, Nanz D, Weishaupt D, Pfammatter T. MR imaging-guided percutaneous sclerotherapy of peripheral venous malformations with a clinical 1.5-T unit: a pilot study. J Vasc Interv Radiol 2009;20:879–887.
4. Boll DT, Merkle EM, Lewin JS. MR-guided percutaneous sclerotherapy of low-flow vascular malformations in the head and neck. Magn Reson Imaging Clin N Am 2005;13:595–600.
5. Hennig J, Nauerth A, Friedburg H. RARE imaging: a fast imaging method for clinical MR. Magn Reson Med 1986;3:823–833.
6. Lauenstein TC, Sharma P, Hughes T, Heberlein K, Tudorascu D, Martin DR. Evaluation of optimized inversion-recovery fat-suppression techniques for T2-weighted abdominal MR imaging. J Magn Reson Imaging 2008;27:1448–1454.
7. Patel MR, Klufas RA, Alberico RA, Edelman RR. Half-fourier acquisition single-shot turbo spin-echo (HASTE) MR: comparison with fast spin-echo MR in diseases of the brain. AJNR Am J Neuroradiol 1997;18:1635–1640.
8. Kiefer B, Grassner J, Hausman R. Image acquisition in a second with half Fourier acquisition single-shot turbo spin-echo. J Magn Reson Imaging 1994;4.
9. Herborn CU, Vogt F, Lauenstein TC, Goyen M, Debatin JF, Ruehm SG. MRI of the liver: can True FISP replace HASTE? J Magn Reson Imaging 2003;17:190–196.
10. Duerk JL, Lewin JS, Wendt M, Petersilge C. Remember true FISP? A high SNR, near 1-second imaging method for T2-like contrast in interventional MRI at .2 T. J Magn Reson Imaging 1998;8:203–208.
11. Paul D, Markl M, Fautz HP, Hennig J. T2-weighted balanced SSFP imaging (T2-TIDE) using variable flip angles. Magn Reson Med 2006;56:82–93.
12. Paul D, Hennig J, Zaitsev M. Intrinsic fat suppression in TIDE balanced steady-state free precession imaging. Magn Reson Med 2006;56:1328–1335.
13. Xu D, Weiss CR, DiCamillo PA, et al.T2-weighted fat suppressed balanced SSFP imaging (contrast-prepared SSFP) for interventional guidance. In: Proc 21st Annual Meeting ISMRM, Salt Lake City; 2013. p 6213.
14. Scheffler K, Heid O, Hennig J. Magnetization preparation during the steady state: fat-saturated 3D TrueFISP. Magn Reson Med 2001;45:1075–1080.
15. Hennig J, Speck O, Scheffler K. Optimization of signal behavior in the transition to driven equilibrium in steady-state free precession sequences. Magn Reson Med 2002;48:801–809.
16. Derbyshire JA, Herzka DA, McVeigh ER. S5FP: spectrally selective suppression with steady state free precession. Magn Reson Med 2005;54:918–928.
17. Griswold MA, Jakob PM, Heidemann RM, et al. Generalized autocalibrating partially parallel acquisitions (GRAPPA). Magn Reson Med 2002;47:1202–1210.
18. Lewin JS, Petersilge CA, Hatem SF, et al. Interactive MR imaging-guided biopsy and aspiration with a modified clinical C-arm system. AJR Am J Roentgenol 1998;170:1593–1601.
19. Lewin JS, Merkle EM, Duerk JL, Tarr RW. Low-flow vascular malformations in the head and neck: safety and feasibility of MR imaging-guided percutaneous sclerotherapy—preliminary experience with 14 procedures in three patients. Radiology 1999;211: 566–570.
20. Flors L, Leiva-Salinas C, Maged I, Hagspiel K. MR imaging of soft-tissue vascular malformations: diagnosis, classification, therapy follow-up. Radiographics 2011;31:1321–1340; discussion 1340–1341.
21. Gold GE, Reeder SB, Yu H, et al. Articular cartilage of the knee: rapid three-dimensional MR imaging at 3.0 T with IDEAL balanced steady-state free precession—initial experience. Radiology 2006;240:546–551.

22. Larson AC, Kellman P, Arai A, Hirsch G, McVeigh E, Li D, Simonetti OP. Preliminary investigation of respiratory self-gating for free-breathing segmented cine MRI. Magn Reson Med 2005;53:159–168.
23. Jarque CM, Bera AK. Efficient tests for normality, homoscedasticity and serial independence of regression residuals. Econ Lett 1980;6:255–259.
24. Montgomery DC. Introduction to factorial designs; the advantages of factorials. In: Design and analysis of experiments. New York: John Wiley & Sons; 2001.
25. Lorenz CH, Kirchberg KJ, Zuehlsdorff S, et al.Interactive frontend (IFE): a platform for graphical MR scanner control and scan automation. In: Proc 12th Annual Meeting ISMRM, Kyoto; 2004. p 2170.
26. Mueller PR, Stark DD, Simeone JF, et al. MR-guided aspiration biopsy: needle design and clinical trials. Radiology 1986;161: 605–609.
27. Weiss CR, Nour SG, Lewin JS. MR-guided biopsy: a review of current techniques and applications. J Magn Reson Imaging 2008; 27:311–325.
28. Lewin JS. Interventional MR imaging: concepts, systems, applications in neuroradiology. AJNR Am J Neuroradiol 1999;20:735–748.
29. Lewin JS, Duerk L, Jain VR, Chao P, Haaga JR. Needle localization in MR-guided biopsy and aspiration: effects of field strength, sequence design, magnetic field orientation. Am J Roentgenol 1996;166:1337–1345.
30. Derakhshan JJ, Nour SG, Sunshine JL, Griswold MA, Duerk JL. Resolution enhanced T(1)-insensitive steady-state imaging. Magn Reson Med 2011 [Epub ahead of print].
31. Srinivasan S, Gilson WD, Flammang AJ, Patil S.Fast, low SAR and off-resonance insensitive T2 weighted variable amplitude PSIF (T2 VAPSIF) imaging. In: Proc 20th Annual Meeting ISMRM, Melbourne; 2012.
32. Miyazaki M, Sugiura S, Tateishi F, Wada H, Kassai Y, Abe H. Non-contrast-enhanced MR angiography using 3D ECG-synchronized half-Fourier fast spin echo. J Magn Reson Imaging 2000;12:776–783.